Chinese Journal of Catalysis 37 (2016) 1324–1330

available at www.sciencedirect.com

ScienceDirect

journal homepage: www.elsevier.com/locate/chnjc

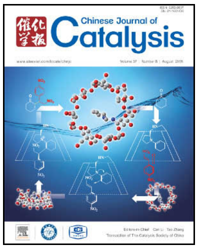

Article

Preparation of a new solid acid and its catalytic performance in di(1-naphthyl)methane hydrocracking

Meixia Zhao, Xianyong Wei *, Zhimin Zong

Key Laboratory of Coal Processing and Efficient Utilization, Ministry of Education, China University of Mining & Technology, Xuzhou 221116, Jiangsu, China

ARTICLE INFO

Article history:
Received 3 March 2016
Accepted 15 April 2016
Published 5 August 2016

Keywords:
Solid acid
Di(1-naphthyl)methane
Hydrocracking
H^+ transfer

ABSTRACT

A new solid acid was prepared by trifluoromethanesulfonic acid (TFMSA) impregnation into an acid-treated attapulgite (ATA). Di(1-naphthyl)methane (DNM) hydrocracking was used as the probe reaction to evaluate the catalytic performance of TFMSA/ATA for cleaving C_{ar}–C_{alk} bridged bonds in coals. The results show that DNM was specifically hydrocracked to naphthalene and 1-methylnaphthalene over TFMSA/ATA in methanol in the absence of gaseous hydrogen. In particular, TFMSA/ATA was demonstrated to be stable after four cycles with slight loss in catalytic activity. Furthermore, a proposed H^+ transfer mechanism successfully interprets the TFMSA/ATA- catalyzed hydrocracking reaction of DNM.

1. Introduction

With decreasing fossil fuel reserves and soaring energy demands, efficient utilization of coals has attracted tremendous attention. Direct coal liquefaction (DCL) is a promising process for producing clean liquid fuels and value-added chemicals [1–3]. In the DCL process, catalysts play crucial roles in cleaving C–C bonds and facilitating hydrogen transfer [4–6]. Liquid acids such as trifluoromethanesulfonic acid (TFMSA) [7,8], $HF+BF_3$ [9], and molten salts [10] have been widely studied in DCL. However, poor recyclability, strong corrosiveness, and the serious environmental contamination issues restrict their industrial applications.

Solid acids are environmentally benign and easily recycled in comparison with liquid acids and have great promise as DCL catalysts. Because of the complexity of coal structures, investigating coal-related model compound (CRMC) reactions proved to be a powerful approach for revealing molecular-level DCL mechanisms [11–13]. In recent years, significant efforts have been devoted to directional degradation of coals and CRMCs over solid acids. Wang et al. [14] investigated the decomposition of diphenylmethane and bibenzyl over sulfated zirconia. The work suggested that the acidic property of the catalyst contributed largely to CRMC bond rupture. Yue et al. [15] examined the hydrocracking of di(1-naphthyl)methane (DNM) over a solid acid prepared by pentachloroantimony and trimethylsilyl trifluoromethanesulfonate impregnation into an activated carbon. The results showed that heterolytic cleavage of H_2 into H^+ and H^- was the key step for the cleavage of C_{ar}–C_{alk} bond in DNM. The aforementioned solid acids, although effective, still require the use of pressurized hydrogen at elevated temperatures. Therefore, it is imperative to develop nov-

---

* Corresponding author. Tel: +86-516-83885951; Fax: +86-516-83884399; E-mail: wei_xianyong@163.com

This work was supported by the Fundamental Research Fund for the Central Universities (China University of Mining & Technology, 2014ZDPY34) and the Priority Academic Program Development of Jiangsu Higher Education Institutions.

DOI: 10.1016/S1872-2067(15)61112-3 | http://www.sciencedirect.com/science/journal/18722067 | Chin. J. Catal., Vol. 37, No. 8, August 2016

el catalysts that allow cleaving the bridged bonds in coals under mild conditions, especially in the absence of pressurized hydrogen.

Catalyst supports play vital roles in improving catalytic activity and stability. Attapulgite is a type of hydrated magnesium aluminum silicate having lath or fibrous morphology, being desirable as a solid acid catalyst support because of its large specific surface area, considerable porosity, and excellent thermal stability [16].

In this study, a new solid acid was prepared using an acid-treated attapulgite (ATA) as the support and TFMSA as the active component. The catalytic performance of as-prepared TFMSA/ATA was investigated by cleaving C_{ar}–C_{alk} bond in DNM in the absence of H_2. The potential cleavage route of DNM over TFMSA/ATA was also deduced.

2. Experimental

2.1. Materials

Attapulgite powder (AP) was purchased from Jiangsu Huahong Mining Chemical Co., Ltd., Xuyi, China. DNM is an analytical reagent purchased from Heowns Chemical Co., Ltd., Tianjin, China. Both methanol and TFMSA were purchased from Aladdin Industrial Inc., Shanghai, China. Methanol was purified by distillation prior to use.

2.2. Catalyst preparation

AP was treated in 0.5 mol/L HCl aqueous solution under reflux with vigorous agitation for 4 h. Thereafter, the suspension was filtered and washed with distilled water until Cl^- was undetectable by silver nitrate titration. The filter cake was dried under vacuum at 110 °C for 6 h to obtain ATA, which was then ground and sieved to 100–200 mesh size. TFMSA/ATA was prepared by impregnation, i.e., TFMSA (5 mL) was added dropwise into ATA (2 g) under a N_2 atmosphere followed by refluxing at 90 °C for 8 h. The mixture was cooled, filtered, washed with acetone, and calcined at 350 °C for 12 h. TFMSA loaded on ATA is ca. 14.7%, which was calculated according to the mass change. Besides TFMSA/ATA, TFMSA/γ-Al_2O_3 and TFMSA/ZSM-5 were also prepared under the same conditions.

2.3. Catalyst characterization

Transmission electron microscopic (TEM) observation of ATA and TFMSA/ATA and corresponding elemental analysis were performed using a JEM-1011 JEOL microscope operating at 200 kV coupled to an energy-dispersive spectrometric detector. Fourier transform infrared (FTIR) analysis was performed using a Nicolet Magna IR-560 spectrometer with a resolution of 4 cm^{-1} over the spectral range of 4000–400 cm^{-1} using KBr pellets. X-ray diffraction (XRD) patterns were recorded on a Bruker D8 Advance diffractometer with Cu K_α radiation (λ = 1.5406 Å) at 40 kV and 30 mA in the 2θ range of 3°–80°. Specific surface area, pore volume, and average pore size of the samples were measured using an Autosorb-1-MP apparatus at −196 °C. Samples were previously outgassed at 300 °C for 5 h. NH_3 temperature-programmed desorption (NH_3-TPD) was conducted on a TP-5000 type multi-function adsorption instrument. The samples were pretreated at 650 °C for 1 h and then cooled to 100 °C. The introduction of NH_3 was performed for 0.5 h followed by purification with He for 1 h to remove physisorbed NH_3. Desorption under He was performed in the range of 100–800 °C at 10 °C/min to remove chemisorbed NH_3. X-ray photoelectron spectroscopic (XPS) measurements were determined using a Thermo Fisher ESCALAB 250Xi spectrophotometer with the Al K_α radiation with a beam spot size of 900 μm (energy step size 1.000 eV, pass energy 50.0 eV). Accurate binding energies were determined by reference to the C 1*s* peak at 284.5 eV.

2.4. Catalytic reactions

DNM (1 mmol), catalyst (0–40 mg), and methanol (10 mL) were added into a 60-mL stainless steel and magnetically stirred autoclave. The autoclave was purged with N_2 and pressurized to 1 MPa at room temperature before heating to a desired temperature (260–320 °C). After reaction at a specific temperature for a prescribed period of time (0.5–5 h), the autoclave was immediately quenched to room temperature in an ice-water bath before filtering the reaction mixture. The filtrate was analyzed using an Agilent 7890/5975 gas chromatograph/mass spectrometer (GC/MS) equipped with a capillary column coated with HP-5MS (60 m × 0.25 mm × 0.25 μm) and a quadrupole analyzer operated in electron impact (70 eV) mode. The capillary column was heated from 60 to 300 °C at 10 °C/min and held at 300 °C for 6 min. The relative content of each compound was determined by normalizing peak area, i.e., the peak area of the compound divided by the sum of the peak areas of all the identified compounds in the total ion chromatogram. Quantitative analysis was performed using DNM as an external standard during analysis with GC/MS. Furthermore, each experiment, under the same conditions, was repeated at least three times to minimize DNM conversion and product yield errors to less than ±1%.

3. Results and discussion

As Fig. 1 shows, ATA exhibits ordered fibrous morphology and a smooth surface with diameters between 20 and 30 nm. Conversely, the surface characteristics of TFMSA/ATA differ from ATA in which a rough surface is observed. Another different surface feature is the presence of irregular grains with diameters < 10 nm that are relatively uniformly distributed on the ATA surface without obvious aggregation. Among the detected elements, O, Mg, Al, and Si are mainly attributed to the ATA framework, while K and Fe most likely arise from impurities in the parent ATA. Additionally, F and S from TFMSA were also detected in TFMSA/ATA (Fig. 2). Energy-dispersive spectrometric (EDS) analysis demonstrates a F content of 5.2 wt% on TFMSA/ATA, which is close to the F loading (5.6%) calculated according to the mass difference between added ATA and the resulting TFMSA/ATA.

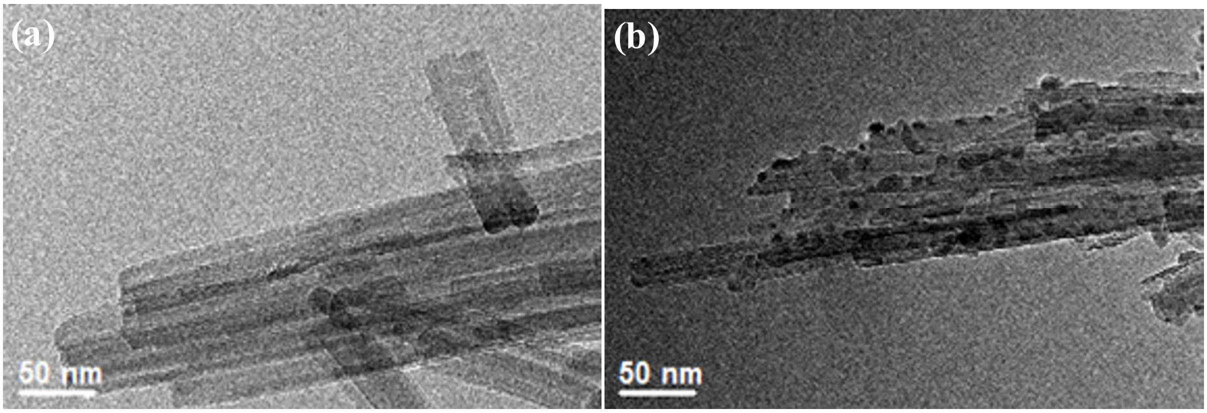

Fig. 1. TEM images of ATA (a) and TFMSA/ATA (b).

As Fig. 3 illustrates, there are significant differences in FTIR spectra among AP, ATA, and TFMSA/ATA. The absorbance at 3616 cm^{-1} is ascribed to the –OH stretching vibration in dioctahedral coordination, while the band at 3550 cm^{-1} is attributed to the –OH stretching vibration of adsorbed water coordinated to Al and Mg at the edges of the channels [17]. The band at 1630 cm^{-1} results from the bending vibration of zeolitic water [18]. The characteristic absorbances at 1015 and 801 cm^{-1} are assigned to Si–OR and Si–O–Si bonds, respectively [19]. Noteworthily, the absorbance of carbonates at 1451 cm^{-1} from ATA and TFMSA/ATA is much weaker than that from AP, indicating that the majority of carbonates in AP were removed by acid treatment. The FTIR spectrum of TFMSA/ATA displays additional bands at 1255 and 1173, 1035, and 614 cm^{-1}, which correspond to symmetric and asymmetric stretching vibrations of the S=O bond, C–F stretching vibrations, and C–S bending vibrations, respectively [20]. These results evidently indicate that TFMSA was successfully loaded on ATA.

As Fig. 4 exhibits, the existence of C, F, S, and O along with other elements in TFMSA/ATA is further verified by XPS analysis. The atomic density of F is ca. 4.40% on the surface of TFMSA/ATA (Table 1), which is consistent with EDS analysis (Fig. 2). The F 1*s* spectrum of TFMSA/ATA is fitted with four distinct peaks related to the various bonding configurations of F atoms in TFMSA/ATA. Specifically, the strong peak located at 687.8 eV is assigned to the F–Al bond [21]. The peak at 688.8 eV is attributed to the F–C bond [22], while the peaks centered at 685.1 and 686.8 eV result from F–Mg and F–Si bonds [23,24], respectively. These results are indicative of the interaction between ATA and supported TFMSA.

As Fig. 5 demonstrates, there are appreciable differences in the XRD patterns among AP, ATA, and TFMSA/ATA. The peaks at 8.5°, 16.9°, and 33.6° can be ascribed to the characteristic diffraction peaks of AP, representing the (110), (040), and (400) planes, respectively, while those at 13.7°, 20.0°, and 21.1° can be attributed to the Si–O–Si crystalline layers in AP [25,26]. The peak at 24.6° can be indexed to the diffraction from quartz as an impurity [27] and its intensity from ATA is much weaker than that from AP, further indicating that the impurity was effectively removed by acid treatment. Compared with ATA, the diffraction peaks of TFMSA/ATA at 8.5°, 16.9°, and 33.6° are weak or broad, implying that the crystalline structure was significantly destroyed by TFMSA loading.

Only a single desorption peak at 358.3 °C was observed in the NH_3-TPD profile of ATA (Fig. 6), which can be assigned to the desorption of NH_3 from medium-strength Lewis acid sites on ATA [28]. Compared with ATA, TFMSA/ATA displays two

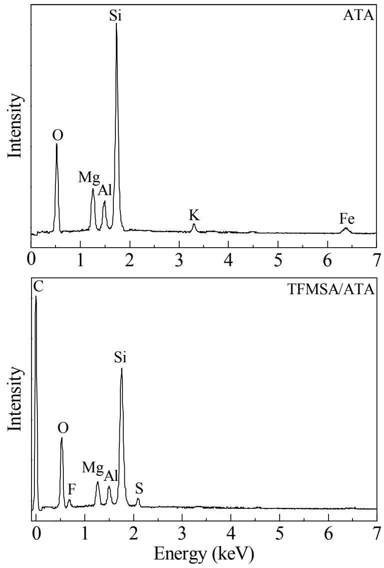

Element	wt %	at %
O K	46.4	60.1
Mg K	6.2	5.3
Al K	5.5	4.2
Si K	40.3	29.7
K K	0.5	0.3
Fe K	1.1	0.4

Element	wt %	at %
C K	34.1	44.7
O K	40.0	39.3
Mg K	2.8	1.8
Al K	2.0	1.2
Si K	13.4	7.5
S K	2.5	1.2
F K	5.2	4.3

Fig. 2. Energy dispersive spectra of ATA and TFMSA/ATA.

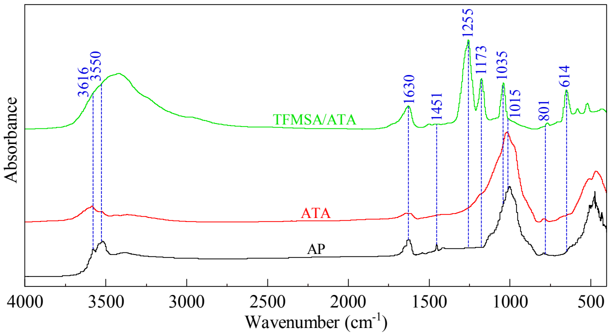

Fig. 3. FTIR spectra of AP, ATA, and TFMSA/ATA.

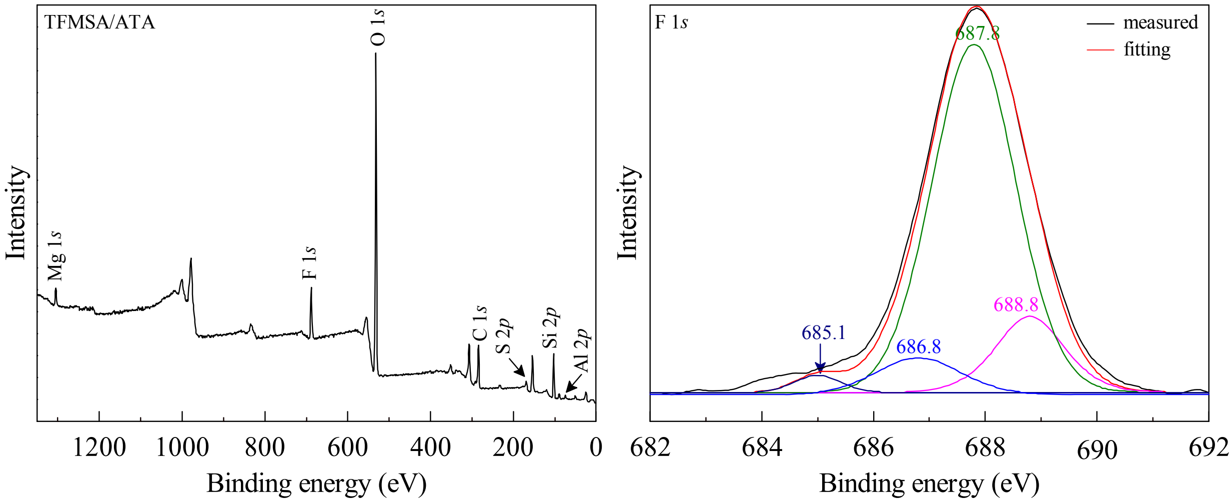

Fig. 4. XPS spectra of TFMSA/ATA.

Table 1
Atomic densities of main elements on the surface of TFMSA/ATA.

Element	Binding energy (eV)	Atomic density (%)
Al 2*p*	74.04	1.13
Si 2*p*	102.70	7.62
S 2*p*	168.55	1.31
C ls	284.17	44.11
O 1*s*	531.94	39.67
F 1*s*	687.86	4.40
Mg 1*s*	1304.82	1.76

desorption peaks at 245.1 and 615.2 °C, indicating the presence of weak and strong acid sites on TFMSA/ATA, respectively. Much stronger acid sites created after supporting TFMSA are tentatively attributed to the interaction of supported TFMSA with ATA, which is responsible for donating H^+.

Table 2 shows that the specific surface area (278 m^2/g) of ATA is significantly larger than that (169 m^2/g) of AP, favoring the subsequent TFMSA loading. The decrease in specific surface area and increase in pore size for ATA after TFMSA loading imply that the majority of TFMSA was anchored to the channels of ATA, expanding the pore size to some extent.

As Fig. 7 exhibits, only naphthalene and 1-methylnaphthalene were detected in the mixtures from DNM hydrocracking, while the resulting formaldehyde from methanol dehydrogenation cannot be detected as it was drawn out together with the solvent during analysis with GC/MS. The results show that both DNM conversion and product yields increase with raising temperature, increasing TFMSA/ATA feed, and prolonging time; however, DNM conversion almost reached 100% at 300 °C over 40 mg TFMSA/ATA for 3 h. Interestingly, the yield of naphthalene is significantly higher than that of 1- methylnaphthalene, indicating significant demethylation of 1-methylnaphthalene. The difference in naphthalene and 1-methylnaphthalene yields also increases with raising temperature, increasing TFMSA/ATA feed, and prolonging time. The data suggest that TFMSA/ATA selectively catalyzes DNM hydrocracking and demethylation of the resulting 1-methylnaphthalene. The activity of TFMSA/ATA for DNM hydrocracking is significantly higher

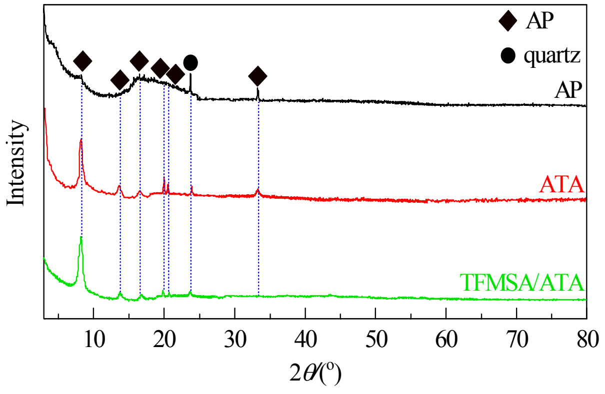

Fig. 5. XRD patterns of AP, ATA, and TFMSA/ATA.

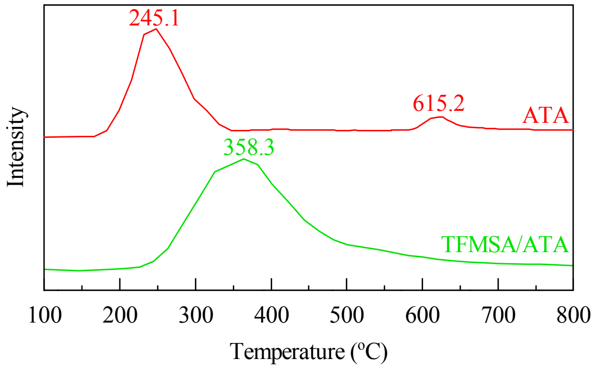

Fig. 6. NH_3-TPD profiles of ATA and TFMSA/ATA.

Table 2
Physicochemical properties of AP, ATA, and TFMSA/ATA.

Sample	Specific surface area (m^2/g)	Pore volume (cm^3/g)	Average pore size (nm)
AP	169	0.29	4.60
ATA	278	0.50	7.55
TFMSA/ATA	156	0.27	7.92

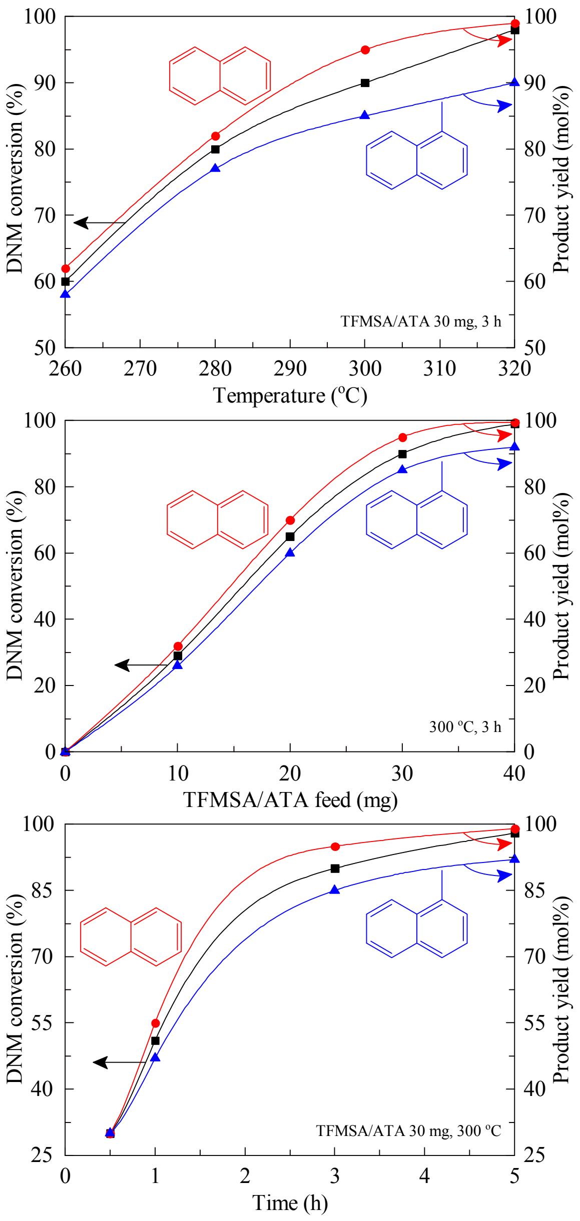

Fig. 7. Effects of temperature, TFMSA/ATA feed, and time on DNM hydrocracking.

than that of either TFMSA/γ-Al_2O_3 or TFMSA/ZSM-5 under the same conditions (Fig. 8). The outstanding catalytic performance displayed by TFMSA/ATA is not only attributed to its large specific surface area but is also related to the synergic effect between ATA and the supported TFMSA.

The dissociation energy of C_{ar}–C_{alk} bond in DNM was reported to be 355.6 kJ/mol, therefore thermal cleavage of the C_{ar}–C_{alk} bond in DNM at 300 °C is extremely difficult [29]. Hydrogen transfer either from $H^•$ or H^+ greatly facilitates C_{ar}–C_{alk} bond cleavage, as the attack of $H^•$ or H^+ on the *ipso*-position of an aromatic ring connected to methylene yields a stable arene rather than a labile aryl radical in addition to a relatively stable leaving group, i.e., an arylmethyl radical or arylmethylium [30,31]. Analysis of TFMSA/ATA suggests that the interaction between ATA and supported TFMSA favors the release of H^+ from TFMSA/ATA. The attack of H^+ from TFMSA/ATA on the *ipso*-position of DNM leads to the formation of naphthalene and naphth-1-ylmethylium, as demonstrated in Scheme 1. Subsequently, H^- abstraction from methanol by the resulting naphth-1-ylmethylium proceeds, resulting in 1-methylnaphthalene and formaldehyde along with the release of H^+. The released H^+ subsequently induces DNM hydrocracking or 1-methylnaphthalene demethylation.

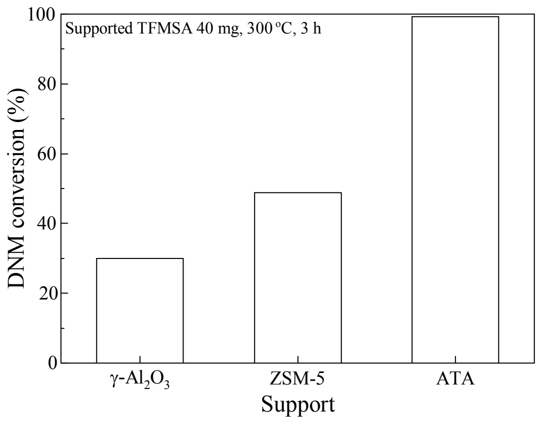

Fig. 8. DNM conversion over different supported TFMSA.

Commercial viability requires excellent catalyst stability, therefore catalytic recycling tests conducted on TFMSA/ATA were performed. As exhibited in Fig. 9, DNM conversion slightly decreases with increasing recycle times, indicating good stability of the catalyst. The slight decrease of DNM conversion may be related to carbon deposition. The NH_3-TPD profile of the recycled TFMSA/ATA catalyst suggests that there is no appreciable loss in acidity for the spent catalyst. The above evidence indicates that TFMSA/ATA presents excellent stability.

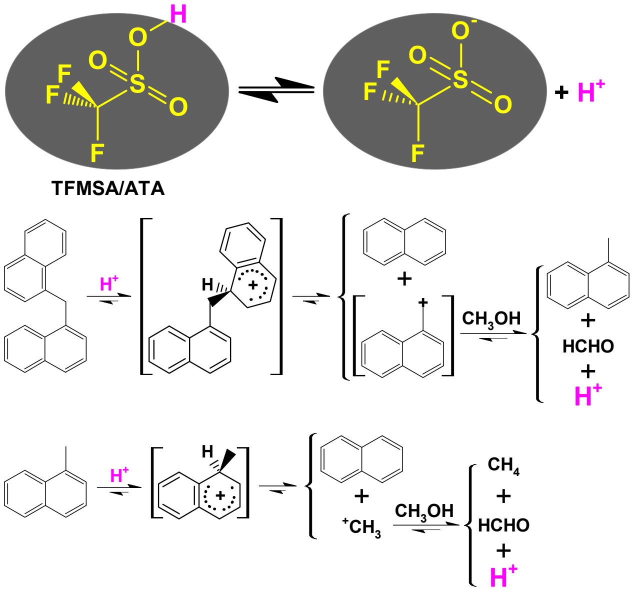

Scheme 1. Possible mechanism for DNM hydrocracking over TFMSA/ATA.

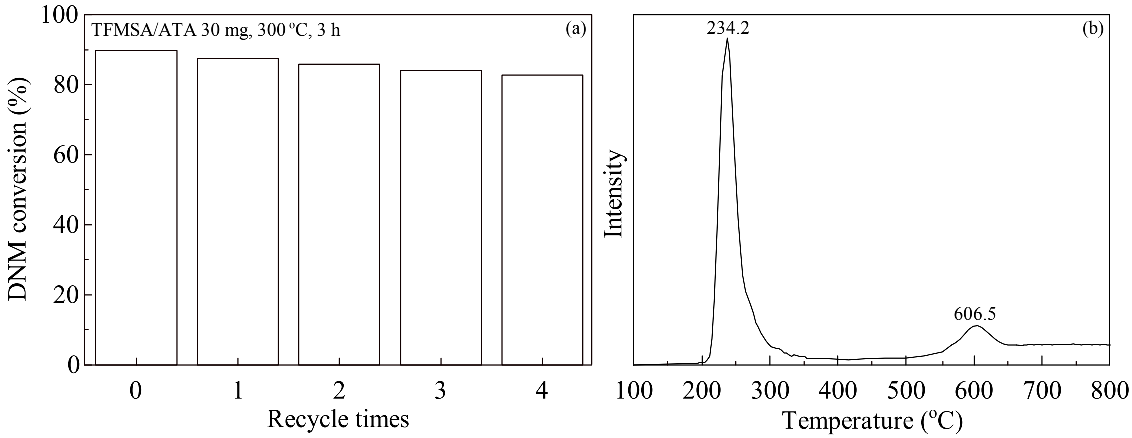

Fig. 9. DNM conversion over fresh and recycled TFMSA/ATA (a) and NH_3-TPD profile of TFMSA/ATA after 4-times of recycles (b).

4. Conclusions

Near 100% hydrocracking of DNM to naphthalene and 1-methylnaphthalene over TFMSA/ATA at 300 °C in methanol in the absence of gaseous hydrogen was observed, suggesting that TFMSA/ATA exhibits excellent catalytic activity for the cleavage of C_{ar}–C_{alk} bridged bonds under mild conditions. The catalytic mechanism of DNM hydrocracking over TFMSA/ATA is ascribed to the preference of the catalyst to promote H^+ transfer to the *ipso*-position of DNM. No obvious deactivation was observed even after several cycles. The TFMSA/ATA catalyst provides a promising new route for preparing similar catalysts applied in coal conversions.

References

[1] S. Vasireddy, B. Morreale, A. Cugini, C. Song, J. J. Spivey, *Energy Environ. Sci.*, **2011**, 4, 311–345.
[2] I. Mochida, O. Okuma, S. H. Yoon, *Chem. Rev.*, **2014**, 114, 1637–1672.
[3] F. Haghighat, A. de Klerk, *Energy Fuels*, **2014**, 28, 1012–1019.
[4] Y. Z. Li, F. Y. Ma, X. T. Su, C. Sun, J. C. Liu, Z. Q. Sun, Y. L. Hou, *Catal. Commun.*, **2012**, 26, 231–234.
[5] X. M. Yue, X. Y. Wei, B. Sun, Y. H. Wang, Z. M. Zong, Z. W. Liu, *Int. J. Min. Sci. Technol.*, **2012**, 22, 251–254.
[6] M. Trautmann, S. Lang, Y. Traa, *Fuel*, **2015**, 151, 102–109.
[7] K. Shimizu, H. Karamatsu, A. Inaba, A. Suganuma, I. Saito, *Fuel*, **1995**, 74, 853–859.
[8] K. Shimizu, K. Miki, I. Saitou, *Fuel*, **1997**, 76, 23–27.
[9] G. A. Olah, M. R. Bruce, E. H. Edelson, A. Husain, *Fuel*, **1984**, 63, 1130–1137.
[10] M. Nomura, T. Muratani, Y. Tajima, S. Murata, *Fuel Process. Technol.*, **1995**, 43, 213–225.
[11] Z. H. Ni, Z. M. Zong, L. F. Zhang, L. B. Sun, Y. Liu, X. H. Yuan, X. Y. Wei, *Energy Fuels*, **2003**, 17, 60–61.
[12] L. B. Sun, Z. M. Zong, J. H. Kou, G. F. Liu, X. Sun, X. Y. Wei, G. J. Zhou, C. W. Lee, *Energy Fuels*, **2005**, 19, 1–6.
[13] M. X. Zhao, X. Y. Wei, M. Qu, Z. K. Li, J. Liu, J. Kong, D. D. Zhang, H. L. Yan, Z. M. Zong, *Fuel Process. Technol.*, **2016**, 142, 258–263.
[14] Z. C. Wang, Z. S. Wang, H. F. Shui, Z. P. Lei, S. B. Ren, S. G. Kang, Y. N. Zhu, *Fuel*, **2010**, 89, 2477–2482.
[15] X. M. Yue, X. Y. Wei, B. Sun, Y. H. Wang, Z. M. Zong, X. Fan, Z. W. Liu, *Appl. Catal. A*, **2012**, 425–426, 79–84.
[16] C. Z. Zhu, X. H. Wang, Q. Huang, L. Huang, J. J. Xie, C. S. Qing, T. H. Chen, *Chem. Eng. J.*, **2013**, 225, 567–573.
[17] H. M. Yang, A. D. Tang, J. Ouyang, M. Li, S. Mann, *J. Phys. Chem. B*, **2010**, 114, 2390–2398.
[18] L. X. Zhang, Q. Z. Jin, L. Shan, Y. F. Liu, X. G. Wang, J. H. Huang, *Appl. Clay Sci.*, **2010**, 47, 229–234.
[19] X. Li, Z. M. Zong, W. W. Ma, J. P. Cao, M. Mayyas, Z. H. Wei, Y. Li, H. L. Yan, D. Wang, R. Yang, X. Y. Wei, *Fuel Process. Technol.*, **2015**, 134,

Graphical Abstract

Chin. J. Catal., 2016, 37: 1324–1330 doi: 10.1016/S1872-2067(15)61112-3

Preparation of a new solid acid and its catalytic performance in di(1-naphthyl)methane hydrocracking

Meixia Zhao, Xianyong Wei*, Zhimin Zong
China University of Mining & Technology

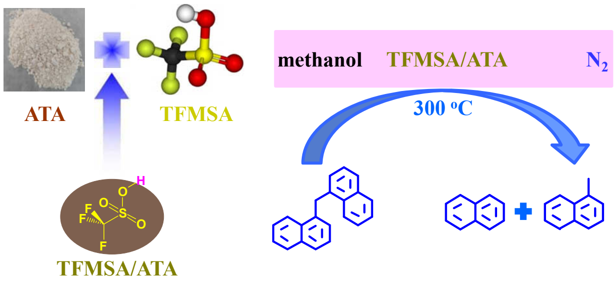

A new solid acid catalyst prepared by trifluoromethanesulfonic acid (TFMSA) impregnation into an acid-treated attapulgite (ATA) specifically hydrocracked di(1-naphthyl)methane to naphthalene and 1-methylnaphthalene over TFMSA/ATA at 300 °C in methanol without gaseous hydrogen.

39–45.

[20] M. Gorsd, L. Pizzio, M. Blanco, *Appl. Catal. A*, **2011**, 400, 91–98.

[21] A. Hess, E. Kemnitz, A. Lippitz, W. E. S. Unger, D. H. Menz, *J. Catal.*, **1994**, 148, 270–280.

[22] C. M. Kassis, J. K. Steehler, R. W. Linton, *Surf. Sci. Spectra*, **1994**, 3, 299–306.

[23] G. E. Murch, R. J. Thorn, *J. Phys. Chem. Solids*, **1980**, 41, 785–791.

[24] H. J. M. Bosman, A. P. Pijpers, A. W. M. A. Jaspers, *J. Catal.*, **1996**, 161, 551–559.

[25] E. Cao, R. Bryant, D. J. A. Williams, *J. Colloid Interface Sci.*, **1996**, 179, 143–150.

[26] D. F. Zhao, J. Zhou, N. Liu, *Mater. Charact.*, **2007**, 58, 249–255.

[27] J. L. Cao, G. S. Shao, Y. Wang, Y. P. Liu, Z. Y. Yuan, *Catal. Commun.*, **2008**, 9, 2555–2559.

[28] L. Rodríguez-González, F. Hermes, M. Bertmer, E. Rodríguez-Castellón, A. Jiménez-López, U. Simon, *Appl. Catal. A*, **2007**, 328, 174–182.

[29] Z. H. Ni, Z. M. Zong, L. F. Zhang, S. L. Zhou, Y. C. Xiong, X. H. Wang, X. Y. Wei, *Energy Fuel*, **2002**, 16, 1154–1159.

[30] M. Farcasiu, C. Smith, *Energy Fuels*, **1991**, 5, 83–87.

[31] E. Ogata, X. Y. Wei, K. Horie, A. Nishijima, I. Saito, K. Ukegawa, *Catal. Today*, **1998**, 43, 161–169.